JP3J.8 MELTING-LAYER CLOUD OBSERVED DURING MR01-K05 CRUISE OF RES/V MIRAI

Kazuaki YASUNAGA[*1], Kunio YONEYAMA[1], Hisayuki KUBOTA[1], Hajime OKAMOTO[2], Atsushi SHIMIZU[3], Hiroshi KUMAGAI[4], Masaki KATSUMATA[1], Nobuo SUGIMOTO[3], and Ichiro MATSUI[3]

[1]Institute of Observational Research for Global Change, JAMSTEC Yokosuka headquarters , Kanagawa, Japan

[2]Center for Atmospheric and Oceanic Studies, Graduate School of Science, Tohoku University, Sendai, Japan

[3]National Institute for Environmental Studies, Tsukuba, Ibaraki, Japan

[4]National Institute of Information and Communications Technology, Tokyo, Japan

1. Introduction

The vertical distribution of radiatively active tracers, aerosols, and clouds influences the earth climate via the radiative properties of the atmosphere. Clouds have the largest radiation-forcing properties. At low latitudes, the short wave flux incident to the top of the atmosphere and long wave radiation flux emitted from the earth surface are large. The vertical distribution of tropical clouds is therefore an important component of understanding the energy balance of Earth.

Over regions of warm tropical sea surface temperatures (SSTs), the atmosphere is conditionally unstable, and many isolated or highly organized convections occur. Johnson et al. (1996) described prominent stable layers at heights of 2 km, 5 km, and 15-16 km, observed during the Tropical Ocean Global Atmosphere Coupled Ocean-Atmosphere Response Experiment (TOGA COARE). Johnson et al. (1999) also found that maxima in the vertical distributions of radar-echo (cloud) tops exist in the vicinity of these three stable layers heights.

It is a well known fact that environmental static stability influences the vertical profiles of detrainment from cumulus convection as well as the top heights of cumulus convection. Yasunaga et al. (2003) performed a statistical analysis of NASA Pacific Exploratory Mission-Tropics B (PEM-Tropics B) observational data and found that tropical cumulus convection directly transported boundary layer air to the 350-600 hPa and 750-800 hPa levels. These pressure levels coincide with the heights where stable layers were frequently observed during the PEM-Tropics B. It is therefore reasonable to expect that clouds detrained from cumulus convection ("detrainment shelves" of Mapes and Zuidema, 1996) would be frequently observed at around the specific layers of 2, 5, and 15-16 km as well as cloud tops.

In the present study, detrainment shelves are considered to be thin cloudy layers composed of small condensate particles of negligible terminal velocity (<0.1 mm in radius). The frequency distribution of thin cloud in the middle troposphere over the tropical western Pacific is examined with the use of 95 GHz cloud profiling radar (wavelength of 3.16 mm) and lidar with a dual wavelength of 532 nm and 1064 nm.

2. Data and meteorological conditions during MR01-K05 Leg3-4 cruise

The data utilized in the present study were obtained by stationary observation over the tropical western Pacific (around 1.85˚N, 138˚E) from November 9 to December 9, 2001 by the Research Vessel Mirai of the Japan Marine Science and Technology Center (JAMSTEC). During the intensive observation period (IOP), the principal mission objectives were C-band weather Doppler radar observations, atmospheric sounding by radiosonde, surface meteorological measurement, conductivity-temperature-depth profiler castings to 500 m, and current measurement by acoustic Doppler current profiler. Additional tasks included turbulent flux measurement, solar radiation measurement, cloud profiling radar (SPIDER), lidar,

*Corresponding author address: Kazuaki Yasunaga, Institute of Observational Research for Global Change, JAMSTEC Yokosuka headquarters, 2-15, Natsushima-Cho, Yokosuka-city, Kanagawa, 237-0061, Japan: E-mail: yasunaga@jamstec.go.jp

and greenhouse gas measurement.

The cloud profiling radar (SPIDER) has a frequency of 95 GHz (wavelength of 3.16 mm). The vertical resolution of the radar data was 82.5 m, with the maximum altitude of the observation being 20 km, with a time resolution of about 0.1 seconds. The radar reflectivity factor is commonly indicated in the logarithmic form (dBZe), and the minimum detectable radar reflectivity factor averaged over 1 minute was –43 dBZe at 5 km. A full description of the cloud profiling radar SPIDER is provided by Horie et al. (2000).

The lidar utilized in the present study is a two-wavelength (532 nm and 1064 nm) Mie-scattering lidar with a depolarization measurement capability of 532 nm. The original data had a vertical resolution of 6 m and a temporal resolution of 10 seconds. The maximum altitude of observations was 20 km. Technical specifications of the lidar are provided by Sugimoto et al. (2001), while additional details concerning the shipborne cloud profiling radar and lidar system are provided by Okamoto et al. (2005).

Figure 1 shows the infrared equivalent blackbody temperature measured during the IOP by Geostationary Meteorological Satellite of the Japan Meteorological Agency. Three active periods of convection were detected: period 1 from 9-14 November 2001, period 2 from 15–28 November 2001, and period 3 from 29 November until 8 December 2001. The timing of period 3 convection corresponds to the active phase of the Madden-Julian Oscillation (MJO), when highly organized convections were observed.

Figure 2 presents time-height cross-sections of zonal and meridional winds derived from radiosonde data. Westerly winds were dominant in the lower troposphere during the entire observational period (Fig. 2a). There were two peaks of strong westerly wind during the middle of November and early December, each time accompanied by cloud activities. The meridional wind component shows the periodic replacement of positive and negative values between the 100 hPa and 300 hPa levels (Fig. 2b), which would indicate that equatorial trapped waves prevailed during this period.

The frequency distribution of temperature lapse rates exceeding the thresholds of -4, -4.5, and -5 K km^{-1} are shown in Fig. 3. The results presented in Fig. 3 were calculated for a depth of 500 m. During the IOP, stable layers were frequently observed at the heights of 2 km and 5.5 km, while weakened stability layers were detected at a height of around 4.5 km (Fig. 3a). The frequency distribution of the height of the stable layer during the IOP is similar to that recorded during TOGA COARE (e.g., Johnson et al. 1996).

The stability at 2 km height became weaker with time, and the stable layer disappeared completely during period 3 (Figs. 3b-d). The stable layer at mid-levels was prominent during all three periods, although the height of the peak was lower (5 km) during period 3 than during periods 1 and 2 (around 5.5 and 6.5 km, respectively). While a layer of weakened stability was observed around 4.5 km height during all three periods, the layer was much shallower during period 3 than during periods 1 and 2.

Figure 4 shows variation in the coverage of C-band radar echoes with reflectivity factors >15 dBZ at 2 km height over a 200 x 200 km area. Radar echo is classified as either convective or stratiform type, following the method by Steiner et al. (1995). During period 1, two major precipitation events occurred (on 9 and 10 November), and stratiform type echoes prevailed. In contrast, precipitation occurred almost daily during period 2, and convective type echoes were dominant, except on 23 November. Period 3 contained the MJO active phase, and coverage of radar echoes was much larger than during periods 1 and 2. Stratiform type echoes were dominant during period 3, which is consistent with the results of Lin et al. (2004).

3. Data analysis and procedures

Radar and lidar data were interpolated to produce consistent vertical and temporal resolution. The combined data used in the present analysis has a vertical resolution of 82.5 m and the time resolution of

1 minute. The base height of cloudy layers with little or no falling condensate particles was determined via the radar reflectivity factor and lidar backscattering coefficient, according to the following three steps.

1. The provisional base level of the cloudy layer (Zl) is defined as the level at which the lidar backscattering coefficient first exceeds a certain threshold (Lc) during a vertical scan from the height of 2 km. The lidar has two wavelengths, and the lower level is selected as Zl. The starting height of the vertical scan, 2 km, was selected in order to avoid aerosols and clouds within the boundary layer.
2. The provisional base level of the cloudy layer (Zr) is defined as the level at which the radar reflectivity factor first exceeds a certain threshold (Rc) during a vertical scan from a height of 2 km.
3. The ultimate base level of the cloudy layer (Zb) is defined by Zl for the case where the height of Zl is less than that of Zr, or where Zl is defined and Zr cannot be determined. Zb is considered to be indefinite in the case of the height of Zr being equal to or lower than that of Zl, or when Zl cannot be determined.

Radar is more sensitive than lidar in terms of falling condensate particles (radius >0.1 mm), and is able to detect such large particles at lower levels than lidar, provided an adequate Rc value is chosen. Therefore, when the height of Zr is equal to or lower than that of Zl, we can conclude that falling condensate particles exist. This forms the basis of defining Zb as indefinite in the third step outlined above. Conversely, lidar is more sensitive to small particles of negligible terminal velocity (<0.1 mm in radius) than radar. Accordingly, when the height of Zl is lower than that of Zr, or when Zr is indefinite, Zl can be considered to represent the base height of a cloudy layer with little or no falling condensate particles. As the absence of falling condensate particles indicates an absence of vigorous diabatic heating within a cloud, the vertical scale of the cloud would not be so large as the convective cloud or the stratiform cloud accompanied by a lot of falling condensate particles.

Figure 5 shows observations made on 10 November 2001. In this case, Lc and Rc are -5.25 (= $\log_{10} \beta$, where β ($m^{-1}\ sr^{-1}$) is the backscattering coefficient) and -35 dBZe, respectively. During 0100-0200 UTC, the lidar backscattering coefficient is large around the height of 5 km, while high radar reflectivity is recorded at lower levels. These observations indicate that condensate particles exist, and that Zb is defined as indefinite (see the lower panel in Fig. 5). In contrast, during 0400-0500 UTC and 2000-2200 UTC, lidar detects thin cloudy layers at mid-levels (5-7 km), while the cloud profiling radar detects only weak (or no) signals. Images from the total sky imager (TSI), a full-color digital imaging and software system designed to automatically monitor cloud conditions, support the existence of a thin cloudy layer (Fig. 6). This example clearly demonstrates the effectiveness of the present analytical method in detecting the base height of thin cloudy layers that do not contain falling condensate particles.

4. Results

Figure 7 shows the frequency distribution of the measured base heights of cloudy layers. Lc varies from -4.25 to -5.25 (= $\log_{10} \beta$, where β ($m^{-1}\ sr^{-1}$) is the backscattering coefficient) at 0.25 intervals, while Rc varies from -10 to -35 dBZe at 5 dBZe intervals. Values averaged over 30 (5 x 6) samples are displayed in Fig. 7. The error bars indicate the ranges within one standard deviation as calculated from the 30 samples.

A peak exists between the heights of 4.5 and 6.5 km during the IOP (Fig. 7a). Although the characteristics of precipitation are different in the three periods (e.g., Fig. 4), the peak is apparent between the heights of 4.5 km and 6.5 km in the all periods (Figs. 7b-d). The mid-level peak apparent in Fig. 7a therefore does not reflect a specific event. The frequent occurrence of the base of cloudy layers around 4.5 – 6.5 km height is presumably a general phenomenon over warm tropical oceans. The heights of the peaks in Fig. 7 do not vary when the starting height of the vertical scan is changed from 0 km to 2 km.

Figures 8 and 9 show examples in which the base of cloudy layers was observed between the heights of 4.5–6.5 km. In Fig. 8, the base of the cloudy layers occurs at mid-levels during 0300–0400 UTC, 1000–1400 UTC, and 1900–2100 UTC. The thickness of observed cloudy layers is relatively thin. Figure 9 shows the occurrence of mid-level thin cloudy layers for almost the entire day. TSI images support the existence of the thin cloudy layers (Fig. 10).

When the base of cloudy layers was detected at around 4.5 – 6.5 km height using the analytical method described in the present study, almost all of the clouds (where clouds are identified as objects with a lidar backscattering coefficient exceeding a certain threshold) had a vertical scale of <500 m. Although attenuation effects prevent lidar from observing structure above the optically thick cloud, the minimal reflectivity of the cloud profiling radar indicates that thick cloudy layers are unlikely to exist above the cloud bases determined from the analytical method described in this study (e.g., Figs 5, 8, and 9). Therefore, the frequency peak of the base heights of mid-level cloudy layers shown in Fig. 7 can be regarded as representing the frequency occurrence of mid-level thin clouds. This interpretation is consistent with the vertical cloud distribution inferred from radiosonde-derived relative humidity data (Mapes and Zuidema, 1996).

References

Horie, H., T. Iguchi, H. Hanado, H. Kuroiwa, H. Okamoto, and H. Kumagai, 2000: Development of a 95-GHz Airborne Cloud Profiling Radar (SPIDER): Technical Aspects, *IEICE Trans. Commun*., E83-B(No.9), 2010- 2020.

Johnson, R.H., P.E. Ciesielski, and K.A. Hart, 1996: Tropical inversions near the 0°C level, *J. Atmos. Sci.*, **53**, 1838-1855.

-, T. M. Rickenbach, S. A. Rutledge, P. E. Ciesielski, and W. H. Schubert, 1999: Trimodal characteristics of tropical convection, *J. Climate*, **12**, 2397-2418.

Lin, J., B. Mapes, M. Zhang, and M. Newman, 2004: Stratiform Precipitation, Vertical Heating Profiles, and the Madden–Julian Oscillation, *J. Atmos. Sci.*, 6**1,** 296–309.

Mapes, B. E., and P. Zuidema, 1996: Radiative-dynamical consequences of dry tongues in the tropical troposphere, *J. Atmos. Sci.*, **53**, 620-638.

Okamoto, H., T. Nishizawa, T. Takemura, H. Kumagai, H. Kuroiwa, N. Sugimoto, I. Matsui, A. Shimizu, A. Kamei, S. Emori, T. Nakajima, Vertical cloud structure observed from shipborne radar and lidar, 2005: Part (I): mid-latitude case study during the MR01/K02 cruise of the R/V *Mirai*, *submitted to J. Geophys. Res.*

Steiner, M., R. A. Houze Jr. and S. E. Yuter. 1995: Climatological Characterization of Three-Dimensional Storm Structure from Operational Radar and Rain Gauge Data. *J. Appl. Meteor.*, **34**, 1978–2007.

Tokay, A., and D. A. Short, 1996: Evidence from tropical raindrop spectra of the origin of rain from stratiform versus convective clouds, *J. Appl. Meteor.*, 35, 355-371

Sugimoto, N., I. Matsui, and A. Shimizu, 2000: Climatological characteristics of cloud distribution and planetary boundary layer structure in Jakarta, Indonesia revealed by lidar observation, *Geophys. Res. Lett.*, **27**, 2909-2912.

Sugimoto, N., I. Matsui, Z. Liu, A. Shimizu, and K. Asai, 2001: Latitudinal distribution of aerosols and clouds in the western Pacific observed with a lidar on board the research vessel Mirai, *Geophys. Res. Lett.*, 28, 4187 -4190.

Yasunaga, K., H.Kida, and T.Satomura, 2003: The 600-750 hPa relative humidity minimum observed during PEM-Tropics B, *Geophysical Research Letters*, 30(24), 2282, doi: 10.1029/2003GL018739.

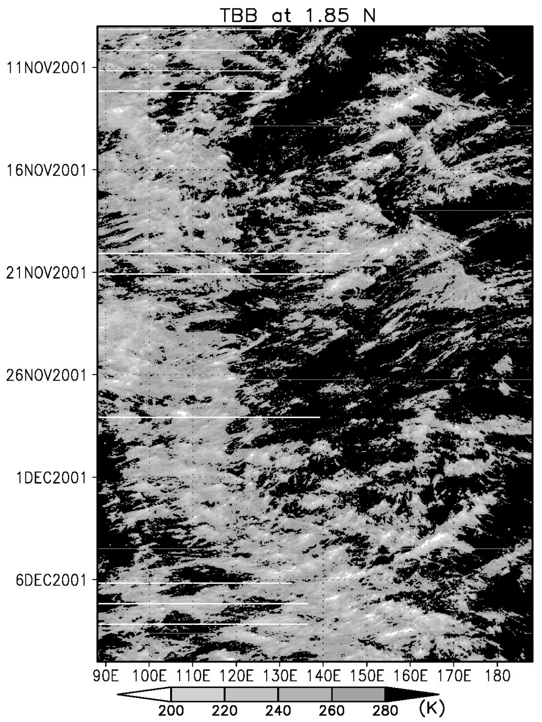

Figure 1: Time-longitude cross-section of infrared equivalent blackbody temperature. Data are from the Geostationary Meteorological Satellite of the Japan Meteorological Agency.

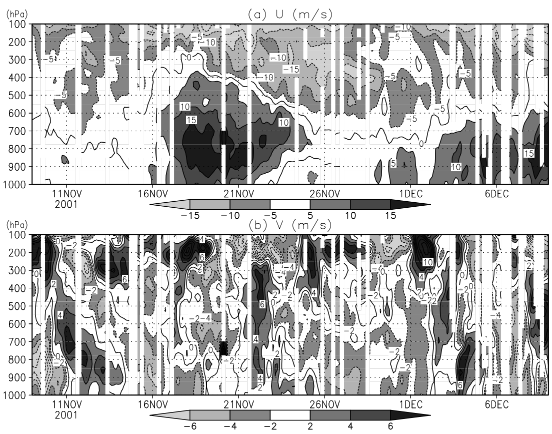

Figure 2: Time-height cross-sections of (a) zonal and (b) meridional wind components derived from radiosonde. Observations were conducted every 3 hours from 0000 UTC, November 9 until 0000 UTC, December 9. Solid and dashed contours indicate positive and negative values, respectively. Periods of no data are left blank.

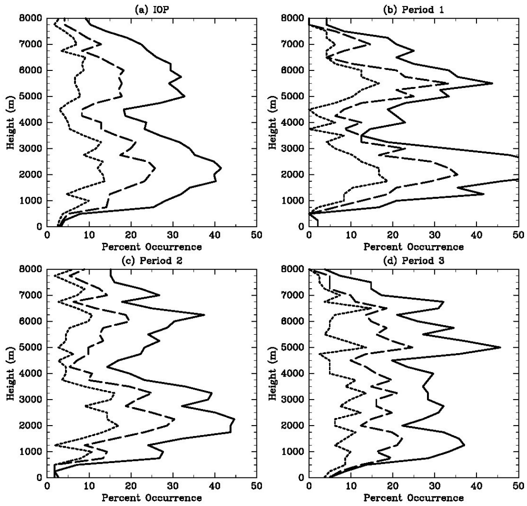

Figure 3: Cumulative frequency of stability (dT/dZ) for values greater than -5 (solid lines), -4.5 (dashed lines), and -4 K km^{-1} (dotted lines) during the IOP (a), period 1 (b), period 2 (c), and period 3 (d).

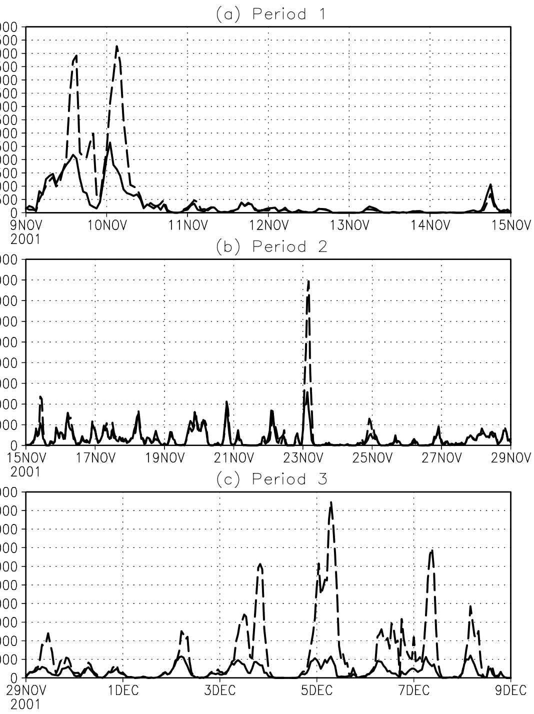

Figure 4: Evolution of the coverage of C-band radar echo for reflectivity factors >15 dBZ at 2 km height over a 200 km x 200 km area during period 1 (a), period 2 (b), and period 3 (c). Solid and dashed lines represent the coverage of convective and stratiform type echoes, respectively.

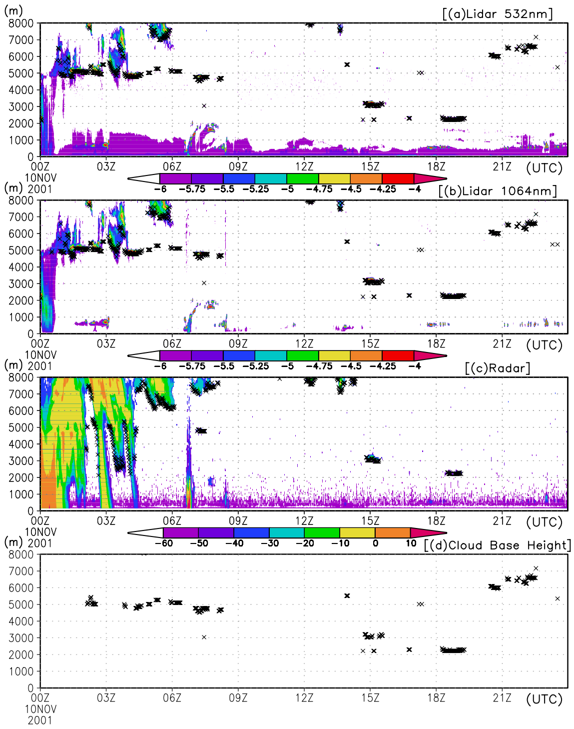

Figure 5: Time-height cross-section of 532 nm lidar backscattering coefficient (a), 1064 nm-lidar backscattering coefficient (b), radar reflectivity factor (c), and ultimate cloud base (Zb) distributions (d). Crosses in the upper three figures indicate the levels where the backscattering coefficient and reflectivity first exceeded certain thresholds during the vertical scan from the height of 2 km.

(a) (b)

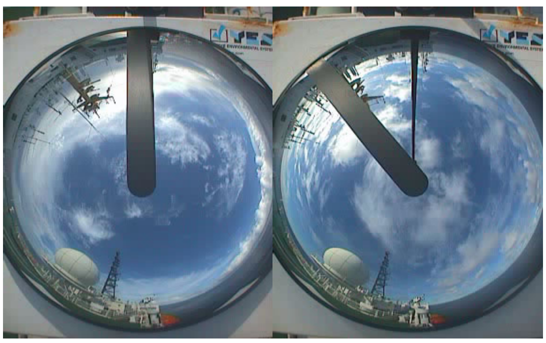

Figure 6: TSI images taken at (a) 0611 UTC, and (b) 2211 UTC on 10 November 2001

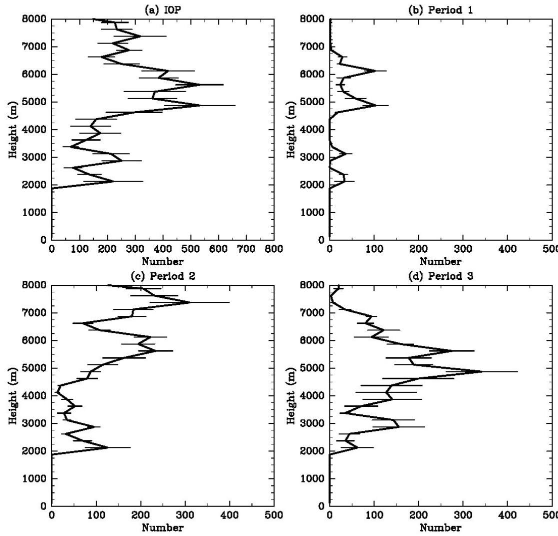

Figure 7: Frequency distribution of the base heights of thin cloudy layers during the IOP (a), period 1 (b), period 2 (c), and period 3 (d). Error bars represent the ranges within one standard deviation calculated from 30 samples.

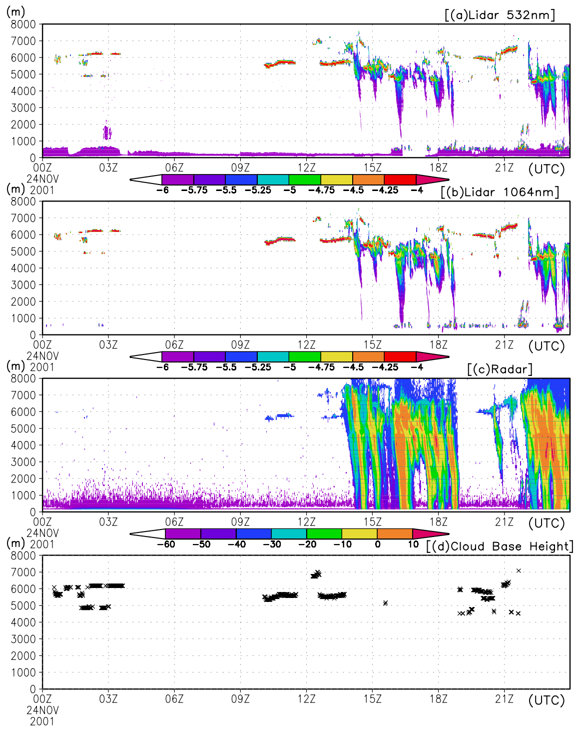

Figure 8: Time-height cross-section of 532 nm lidar backscattering coefficient (a), 1064 nm lidar backscattering coefficient (b), radar reflectivity factor (c), and ultimate cloud base (Zb) distributions (d) on 24 November 2001.

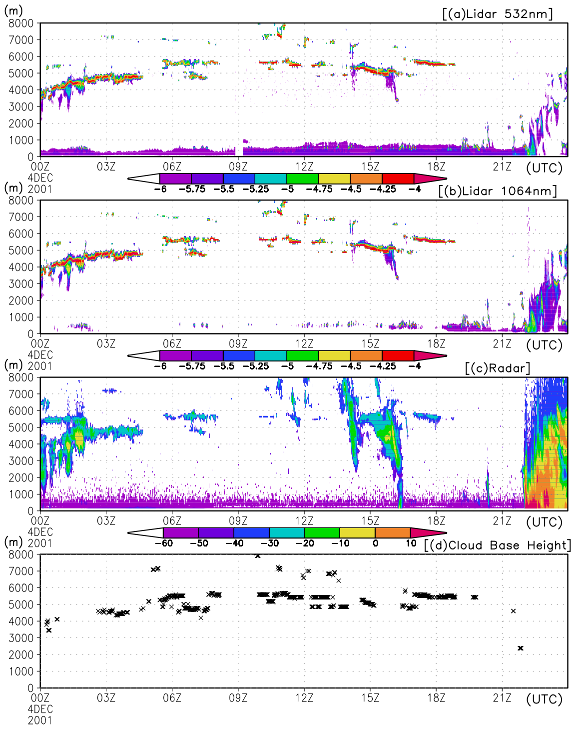

Figure 9: The same as Fig. 8, except on 4 December 2001.

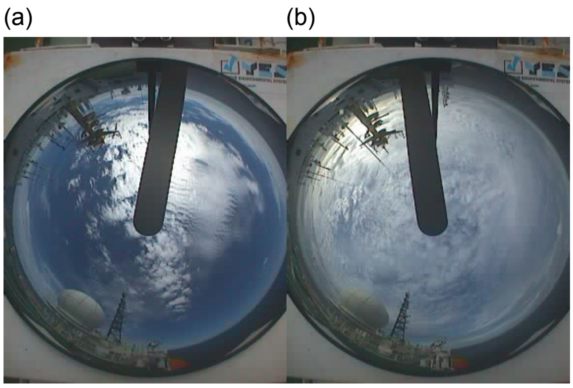

Figure 10: TSI images taken at (a) 0041 UTC on 24 November, and (b) 0711 UTC on 4 December 2001